



HAL
open science

Coherent coupling of individual quantum dots measured with phase-referenced two-dimensional spectroscopy: Photon echo versus double quantum coherence

Valentin Delmonte, Judith F. Specht, Tomasz Jakubczyk, Sven Hofling, Martin Kamp, Christian Schneider, Wolfgang Langbein, Gilles Noguees, Marten Richter, Jacek Kasprzak

► To cite this version:

Valentin Delmonte, Judith F. Specht, Tomasz Jakubczyk, Sven Hofling, Martin Kamp, et al.. Coherent coupling of individual quantum dots measured with phase-referenced two-dimensional spectroscopy: Photon echo versus double quantum coherence. *Physical Review B*, 2017, 96 (4), pp.041124(R). 10.1103/PhysRevB.96.041124 . hal-01629962

HAL Id: hal-01629962

<https://hal.science/hal-01629962>

Submitted on 16 Mar 2022

HAL is a multi-disciplinary open access archive for the deposit and dissemination of scientific research documents, whether they are published or not. The documents may come from teaching and research institutions in France or abroad, or from public or private research centers.

L'archive ouverte pluridisciplinaire **HAL**, est destinée au dépôt et à la diffusion de documents scientifiques de niveau recherche, publiés ou non, émanant des établissements d'enseignement et de recherche français ou étrangers, des laboratoires publics ou privés.

Coherent coupling of individual quantum dots measured with phase-referenced two-dimensional spectroscopy: photon echo versus double quantum coherence

Valentin Delmonte,^{1,2} Judith F. Specht,³ Tomasz Jakubczyk,^{1,2} Sven Höfling,⁴ Martin Kamp,⁴ Christian Schneider,⁴ Wolfgang Langbein,⁵ Gilles Nogues,^{1,2} Marten Richter,³ and Jacek Kasprzak^{1,2,*}

¹*Univ. Grenoble Alpes, F-38000 Grenoble, France*

²*CNRS, Institut Néel, "Nanophysique et semiconducteurs" group, F-38000 Grenoble, France*

³*Institut für Theoretische Physik, Nichtlineare Optik und Quantenelektronik, Technische Universität Berlin, Hardenbergstrasse 36, 10623 Berlin, Germany*

⁴*Technische Physik, University of Würzburg, Würzburg, Germany*

⁵*School of Physics and Astronomy, Cardiff University, The Parade, Cardiff CF24 3AA, United Kingdom*

(Dated: November 17, 2021)

We employ two-dimensional (2D) coherent, nonlinear spectroscopy to investigate couplings within individual InAs quantum dots (QD) and QD molecules. Swapping pulse ordering in a two-beam sequence permits to distinguish between rephasing and non-rephasing four-wave mixing (FWM) configurations. We emphasize the non-rephasing case, allowing to monitor two-photon coherence dynamics. Respective Fourier transform yields a double quantum 2D FWM map, which is corroborated with its single quantum counterpart, originating from the rephasing sequence. We introduce referencing of the FWM phase with the one carried by the driving pulses, overcoming the necessity of its active-stabilization, as required in 2D spectroscopy. Combining single and double quantum 2D FWM, provides a pertinent tool in detecting and ascertaining coherent coupling mechanisms between individual quantum systems, as exemplified experimentally.

Nuclear magnetic resonance (NMR) spectroscopy conceived phase-locked, multi-pulse techniques, yielding multi-dimensional spectra by Fourier transforming temporal sequences into respective frequency coordinates [1, 2]. The possibility to spread the response of biological or chemical molecules of high structural complexity, especially proteins, across many axes enabled to assess their spatial form and to understand inter-atomic interactions and couplings. The idea to selectively address and evolve subsets of transitions from congested spectra via multi-pulse toolbox, and then projecting the results onto two-dimensional (2D) or three-dimensional diagrams, is a far-reaching legacy of NMR. As concern optical spectroscopy, achieving phase-stabilized sequences of laser pulses is more challenging, owing to substantially shorter optical cycles with respect to radio-frequency domain used in NMR. Thus, it has been first accomplished in mid-NIR regime [3–5] and recently conveyed into NIR-VIS range [6–10], while being continuously improved employing active pulse-shaping [11–13] and phase-feedback techniques [14, 15].

At a juncture of coherent spectroscopy and condensed matter physics, 2D spectroscopy provided insight into dynamics and couplings of many-body optical excitations in solids, in particular of excitons in semiconductor quantum wells [11, 12, 16] and novel 2D layered materials [17], as well as in ensembles of quantum dots [18, 19] (QDs) or nanocrystals [20]. A principal tool in these investigations is k-resolved four-wave mixing (FWM) spectroscopy and its extensions probing multi-wave mixing processes [12]. FWM microscopy of single QD excitons [21] was accomplished by phase-sensitive optical heterodyning combined

with interferometric detection, efficiently subtracting resonant background and permitting co-linear geometry of the excitation pulses. Recently, detection sensitivity of intrinsically weak single QD FWM has been enhanced substantially by using photonic nanostructures, improving the QD coupling with external laser beams [22–24].

Here, we perform FWM spectroscopy of individual InAs QDs embedded in a low-Q semiconductor microcavity [2, 22, 25]. We point out two major advancements: Firstly, we demonstrate 2D FWM constructed from two-photon coherences — known as double quantum 2D FWM [27–29] — driven on individual transitions, specifically QD exciton-biexciton systems (GXB) [30]. Secondly, we introduce referencing of the FWM phase, offering convenient alternative for its active-stabilization, which is widely believed to be required in 2D spectroscopy. Using the one-quantum and two-quantum spectroscopy, we have measured single QDs and a QD molecule. A comparison of the spectra signatures to theory allowed us to identify the nature of the internal coupling mechanism in the QD molecule system. Our work shows that the combined single and double quantum 2D spectroscopy is a powerful tool to reveal and understand coherent coupling and excitation transfer mechanisms - an interdisciplinary issue spanning from biology and photo-chemistry, to quantum engineering. The results are especially pertinent for the latter area, as we open new avenues of research in quantum control of optically active nanoscopic two-level and few-level systems in solids.

To acquire the FWM spectra [22], we use a pair of 100 fs laser pulses: \mathcal{E}_1 and \mathcal{E}_2 , with a variable delay τ_{12} , posi-

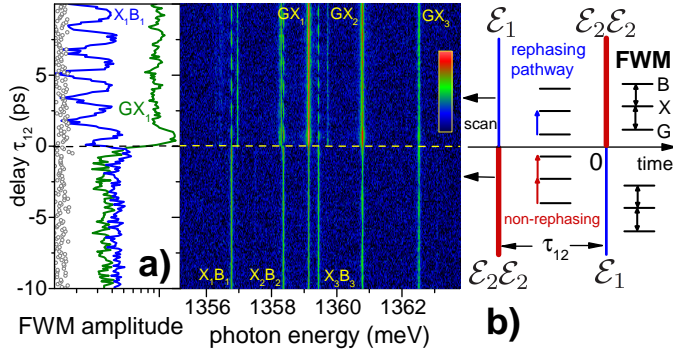


FIG. 1. **Rephasing and non-rephasing pathways in two-beam four-wave mixing.** (a) Typical measurement of the FWM amplitude as a function of τ_{12} on a few InAs QDs embedded in a low-Q microcavity. Impinging \mathcal{E}_1 , \mathcal{E}_2 intensities of (150, 600) nW correspond to pulse areas of around $(0.4\pi, 0.8\pi)$, significantly beyond the $\chi^{(3)}$ limit. Positive (negative) delays τ_{12} corresponds to rephasing (non-rephasing) FWM pathways, as depicted in b).

tive for \mathcal{E}_1 leading. They are frequency shifted by Ω_1 and Ω_2 , respectively, using acousto-optic deflectors. FWM heterodyne beat with a reference field \mathcal{E}_R is retrieved at $2\Omega_2 - \Omega_1$ frequency, carrying the lowest order response $\mathcal{E}_1^* \mathcal{E}_2 \mathcal{E}_2$ (where \star denotes complex conjugate) and also higher orders with the same phase evolution. The signal is spectrally dispersed using a spectrometer, detected with a CCD camera and retrieved in amplitude and phase by applying spectral interferometry.

As shown in Fig. 1 b, in two-beam FWM, the first pulse \mathcal{E}_1 induces coherence, which evolves during τ_{12} , to be then converted into FWM by the second pulse \mathcal{E}_2 , arriving a few picoseconds after \mathcal{E}_R . The lowest electronic excitations of a neutral QD can be cast into three categories of states: a ground state (G), single excitons (X) and two-exciton states, known as biexcitons (B). GX transitions are addressed by one-photon coherence driven by \mathcal{E}_1 , which is converted to FWM of GX and XB by a density grating $\mathcal{E}_1^* \mathcal{E}_2$ on G and X [2, 9]. Inverting temporal ordering of the two light pulses, GB transition can be inspected by a two-photon coherence induced by \mathcal{E}_2 , transformed into FWM of both transitions at the arrival of \mathcal{E}_1 [2, 9]. The simple three-level system of Fig. 1 b illustrates the case of a neutral QD driven along one of its polarization axes. For a single two-level system, like a QD trion, FWM can be only created for $\tau_{12} > 0$ from one-photon coherence induced by \mathcal{E}_1 , since the trion system cannot be doubly excited within the employed spectral bandwidth. In fact, two transitions in Fig. 1 a show strictly no signal for $\tau_{12} < 0$ and are attributed to trion transitions. Therein, we also recognize pairs of exciton-biexcitons, labeled as: $GX_1 - X_1B_1$, $GX_2 - X_2B_2$, $GX_3 - X_3B_3$ occurring in three distinct QDs. FWM exhibits a pronounced beating as a function of $\tau_{12} > 0$, with a period corresponding to B binding en-

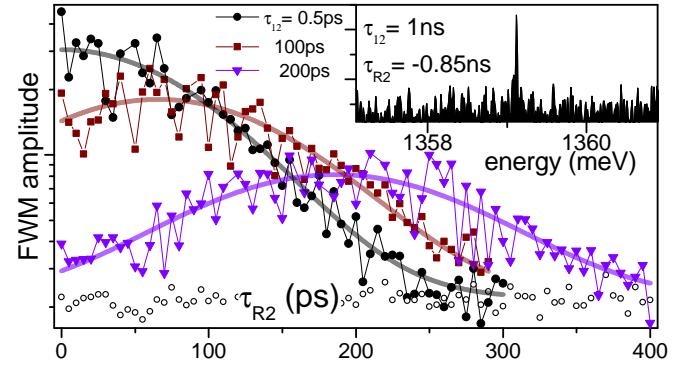


FIG. 2. **Photon-echo formation on a single QD exciton measured upon FWM rephasing pathway** τ_{R2} is scanned for different values of τ_{12} , as indicated. Temporal width of the echo yields inhomogeneous broadening σ .

ergy, which is induced beyond $\chi^{(3)}$ regime by high order contributions propagating at the FWM frequency [2, 32]. Instead, for $\tau_{12} < 0$ FWM is equally created on GX and XB transitions, with no beating.

Time-resolved FWM transient created upon the two pulse configurations displays different characteristics. For $\tau_{12} > 0$, there is a phase-conjugation between \mathcal{E}_1 and FWM. Owing to the rephasing, FWM of an inhomogeneously broadened system has a Gaussian form, with a maximum at $t = \tau_{12}$ and temporal width inversely proportional to the probed spectral inhomogeneous broadening σ . Importantly, time-integrated amplitude of such photon echo is not sensitive on σ , instead the homogeneous broadening is probed through the τ_{12} -dependence. At a level of individual transitions, σ is accumulated due to a residual spectral wandering in time-averaged measurement [9, 23, 24, 33]. For σ in μeV range, which is a case even for high quality QD systems, the echo width becomes comparable or larger than the temporal sensitivity, given by the spectrometer resolution (here about 120 ps). To demonstrate formation of such a broad echo [24], we scan the delay τ_{R2} , between \mathcal{E}_R and \mathcal{E}_2 , for three different τ_{12} , as shown in Fig. 2. The echo develops fully only for $\tau_{12} = 200$ ps, from its width (FWHM) $t_\sigma = \hbar/\sigma = (214 \pm 33)$ ps we retrieve spectral inhomogeneous broadening $8 \ln(2)\sigma = 8 \ln(2)\hbar/t_\sigma = (17 \pm 3) \mu\text{eV}$ (FWHM). Adjusting τ_{R2} permits to retrieve FWM significantly beyond the temporal resolution of the setup, as shown in the inset for $\tau_{12} = 1$ ns.

For $\tau_{12} < 0$ there is no strict phase conjugation between two-photon coherence and FWM, and therefore the photon echo is absent. In Fig. 3 c we show FWM(t, τ_{12}) maps measured on GX_1 and X_1B_1 transitions. As τ_{12} is increased towards more negative values, FWM decay becomes more pronounced, owing to a non-rephasing character of the signal. The two-photon coherence dynamics of GX_1 and X_1B_1 , i.e. respective time-integrated FWM versus τ_{12} , are presented in Fig. 3 a and b. From

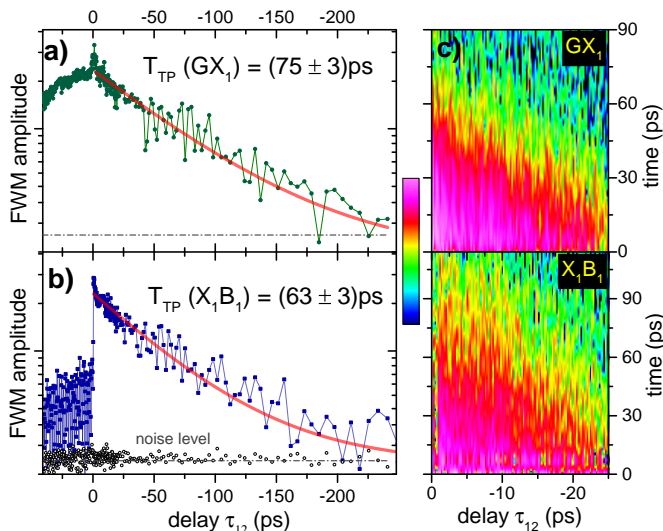


FIG. 3. Two-photon coherence dynamics and two-photon dephasing of GX_1 and X_1B_1 measured at the non-rephasing FWM configuration, $\tau_{12} < 0$.

the exponential decay we retrieve two-photon dephasing $T_{TP}(GX_1, X_1B_1) = (75 \pm 3, 65 \pm 3)$ ps. Similar values of T_{TP} are retrieved by analyzing two other GX - XB pairs.

To illustrate couplings in the probed system of a few QDs, we Fourier-transform FWM(ω_3, τ_{12}) sequences with respect to the delay τ_{12} . The experimental setup is encapsulated, providing a passive stabilization of the phase during the acquisition. However, the phase relationship between FWM measured for subsequent τ_{12} is inevitably lost and can only be achieved via active-stabilization [14, 15], which is not implemented here. The knowledge of the FWM phase for subsequent delays τ_{12} is a precondition to execute the Fourier transform yielding 2D FWM. In our previous works [2, 4], we have circumvented this issue by imposing a phase relationship onto the data by choosing a separated transition in the spectral domain, acting as a local oscillator, and setting its phase to zero for all delays. We then applied this phase factor globally to the full spectrum, adjusting all other frequencies versus τ_{12} , accordingly. Such transformation remains justified, as long as the guiding transition to correct for, in particular exhibiting no coherent coupling, is available in the spectrum. This generally might not be the case. To overcome this experimental limitation, we have conceived a post-treatment protocol permitting to reference the FWM phase, using auxiliary spectral interferences of \mathcal{E}_R with the driving pulses, as explained in Supplementary Material.

In Fig. 4 we present 2D FWM obtained from the set of QDs highlighted in Fig. 1. For $\tau_{12} > 0$, FWM generated by all resonances driven by \mathcal{E}_1 , forms a diagonal in the resulting 2D spectrum. This includes, single trions and neutral excitons, but also biexcitons - the latter can di-

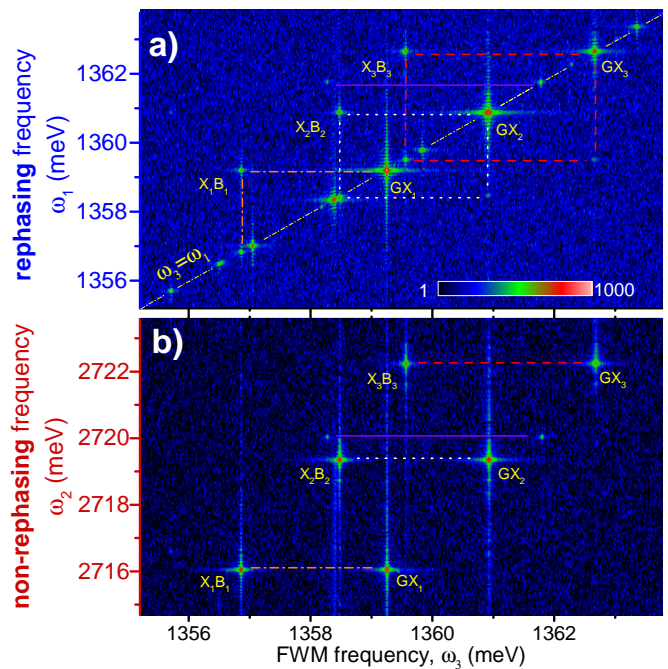


FIG. 4. Two-dimensional FWM spectroscopy of exciton complexes in a few InAs QDs probed along the rephasing (a) and non-rephasing (b) pathways. Four exciton-biexciton systems in different QDs are indicated by dash-dotted, dotted, dashed and solid lines, respectively.

rectly be driven by \mathcal{E}_1 beyond the $\chi^{(3)}$ limit [2], as applied here (an example in the $\chi^{(3)}$ limit is provided in the Supplementary Fig. S6). The biexcitons are off-diagonally shifted by their respective binding energies of a few meV, and form square-like features in 2D FWM under strong excitation, i.e. close to $(\pi/2, \pi)$ area of $(\mathcal{E}_1, \mathcal{E}_2)$ pulses. 2D FWM resulting from $\tau_{12} < 0$ is shown in Fig. 4 b. FWM originates from a corresponding two-photon resonance driven by \mathcal{E}_2 . Here, the two-photon energy corresponds to the sum GX and XB transition energies. In such non-rephasing 2D FWM, we retrieve the response of GXB systems, whereas exciton complexes without doubly excited states within the excitation bandwidth, such as singly charged QDs, do not contribute.

Fig. 5 a and c show the measured rephasing and non-rephasing 2D spectra recorded at another position at the sample. In the following, we focus on the two QDs that show up as transitions GX_1 and GX_2 on the diagonal of the rephasing spectrum with resonance energies $E_1=1359.7$ meV and $E_2=1358.95$ meV - via hyperspectral imaging [4] these are found to be within $0.5 \mu\text{m}$ vicinity (see Supplementary Fig. S7). The peak pattern highlighted by the dashed lines differs from the signatures observed in Fig. 4 in two major respects: First, spin-orbit coupling of the two circularly polarized excitons within each QD leads to linearly polarized exciton eigenstates, where each QD is described by a four-level

system [2]. This causes a splitting of each exciton resonance on the diagonal of the rephasing spectrum into clusters of four peaks. Second, besides the X_1B_1 and X_2B_2 peaks that are redshifted along the FWM axis by the intradot biexciton binding energies $\Delta_1 = -3.3$ meV and $\Delta_2 = -3.6$ meV, respectively, we observe two off-diagonal cross peaks labeled X_2X_1 and X_1X_2 at the spectral positions ($\omega_3 = E_2; \omega_1 = E_1$) (upper cross peak) and ($\omega_3 = E_1; \omega_1 = E_2$) (lower cross peak). The appearance of these cross peaks clearly indicates a coherent interdot coupling between the two QDs: The electrostatic Coulomb coupling leads to an energy renormalization of the interdot biexciton B_{12} consisting of one exciton in each QD. The biexciton shift lifts the symmetry of the lower GX_1 (GX_2) and higher X_1B_{12} (X_2B_{12}) transitions such that the quantum pathways involving these transitions do not destructively interfere anymore and cross peaks show up [4]. A level scheme of such a QD molecule including all coupling-induced energy shifts is shown in Supplementary Fig. 1. The electrostatic interaction Δ_{12} between two excitons located in two different QDs is small compared to the intradot biexciton binding energies. In fact, spectrally-resolved FWM amplitude, shown in the Supplementary Fig. S7, reveals that it is only of the order of $\Delta_{12} = 90 \mu\text{eV}$ and it shifts the interdot biexciton towards higher energies, showing up as blueshifted high-energy shoulders of the exciton resonance peaks. This interpretation is supported by calculations [1] (see Supplementary Material) of the rephasing and non-rephasing 2D signals depicted in Fig. 5 b and d.

In the non-rephasing two-quantum spectrum, the coupling of the two QDs manifests itself in a peak pair labeled X_1B_{12} and X_2B_{12} at the interaction-shifted two-exciton transition GB_{12} (energy $\omega_2 = E_1 + E_2 + \Delta_{12} = 2718.74$ meV) with FWM frequencies $\omega_3 = E_1 = 1359.7$ meV and $\omega_3 = E_2 = 1358.95$ meV, respectively. Theoretical calculations also suggest that exciton transfer processes between the two QDs such as dipole-induced (Förster) interaction and Dexter-type coupling via wave-function overlap are negligible [36]: First, these coupling types are expected to be in the μeV range [4] and therefore difficult to detect at our spectrometer resolution of $25 \mu\text{eV}$. Second, they would lead to additional peaks for an intradot biexciton in one QD after the first pulse has created a single-exciton in the other QD. These peaks are not observed in the spectra indicating that exciton transfer elements are negligible, as elaborated in the Supplementary Material (Fig. S3).

An interesting feature about the observed QD molecule is that, in contrast to the other isolated exciton-biexciton systems, the two coupled QDs show a pronounced fine-structure splitting (FSS) of the order of $60 \mu\text{eV}$ and $140 \mu\text{eV}$, respectively. This is around 5 times higher than the FSS typically present in these QDs [2]. Moreover, the FSS of the other isolated exciton-biexciton systems in our sample (see also Fig. 4) is not visible since the direction

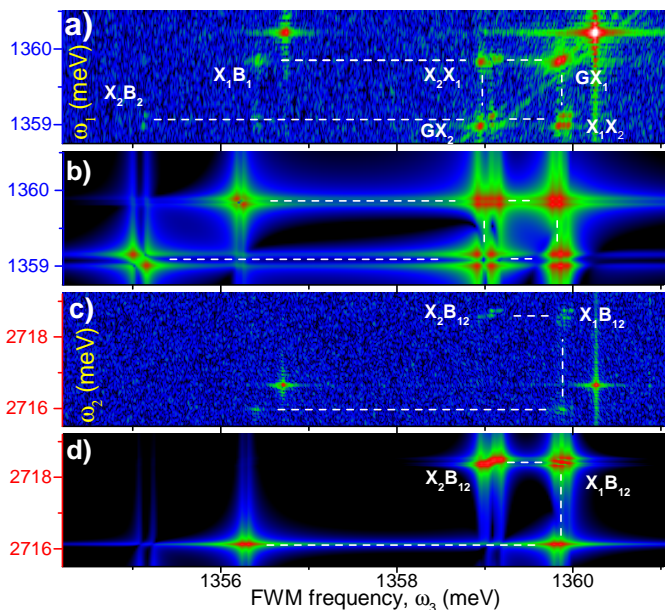


FIG. 5. **Quantum dot molecule, consisting of two electrostatically coupled InAs QDs, observed in single and double quantum 2D FWM.** Measured rephasing (a) and non-rephasing (c) 2D FWM spectra revealing coherent couplings between two QDs. Corresponding simulations are shown in (b) and (d) with the parameters as listed in the Supplementary Material. The signatures belonging to this QD molecule are marked by dashed lines. Additional exciton-biexciton pair in (a) and (c) at (1360.3, 1356.8) meV occurs in other QD, not involved in the molecule formation, thus not included in the calculated spectra.

of the linear excitation/reference polarization was chosen to be parallel to the anisotropy axis. The observation of such a pronounced FSS only for the resonances associated with the QD molecule therefore suggests that the spatial proximity of the two coupled QDs altered the local symmetry of the confinement, changing the magnitude of the FSS and the polarization of the excitonic transitions.

In summary, we have implemented phase-referenced double quantum 2D FWM spectroscopy of individual quantum systems. By merging it with the single quantum counterpart, we have ascertained coherent couplings between excitons, optical selection rules, the structure of (bi-)exciton states, and coupling energies in single InAs QDs and in a quantum dot molecule. This methodology is appealing to infer electronic couplings and charge transfer in deterministically defined QD molecules [37, 38] and propagative coherence in photonic molecules [39]. By merging it with recently developed multi-wave mixing toolbox [22], it could be also used to visualize and control polaritonic couplings in solid state cavity-quantum electrodynamics [40].

ACKNOWLEDGEMENTS

We gratefully acknowledge the financial support by the European Research Council (ERC) Starting Grant PIC-SEN (grant no. 306387). J.S. and M.R. acknowledge financial support by SFB 787 and GRK 1558.

* jacek.kasprzak@neel.cnrs.fr

- [1] Wüthrich, K. Nobel Lecture: NMR studies of structure and functions of biological macromolecules. *Journal of Biomolecular NMR* **27**, 13 (2003).
- [2] Vandersypen, L. M. K. & Chuang, I. L. NMR techniques for quantum control and computation. *Rev. Mod. Phys.* **76**, 1037 (2005).
- [3] Hamm, P., Lim, M. & Hochstrasser, R. M. Structure of the amide I band of peptides measured by femtosecond nonlinear-infrared spectroscopy. *J. Phys. Chem. B* **102**, 6123–6138 (1998).
- [4] Mukamel, S. Multidimensional femtosecond correlation spectroscopies of electronic and vibrational excitations. *Annu. Rev. Phys. Chem.* **51**, 691 (2000).
- [5] Réhault, J. et al. 2D IR spectroscopy with phase-locked pulse pairs from a birefringent delay line. *Opt. Express* **22**, 9063–9072 (2014).
- [6] Brixner, T., Stiopkin, I. V. & Fleming, G. R. Tunable two-dimensional femtosecond spectroscopy. *Opt. Lett.* **29**, 884 (2004).
- [7] Brixner, T., Mančal, T., Stiopkin, I. V. & Fleming, G. R. Phase-stabilized two-dimensional electronic spectroscopy. *J. Chem. Phys.* **121**, 4221 (2004).
- [8] Brixner, T. et al. Two-dimensional spectroscopy of electronic couplings in photosynthesis. *Nature* **434**, 625 (2005).
- [9] Collini, E. et al. Coherently wired light-harvesting in photosynthetic marine algae at ambient temperature. *Nature* **463**, 644–648 (2010).
- [10] Brańczyk, A. M., Turner, D. B. & Scholes, G. D. Crossing disciplines - A view on two-dimensional optical spectroscopy. *Ann. Phys.* **526**, 31–49 (2014).
- [11] Stone, K. W. et al. Two-quantum 2D FT electronic spectroscopy of biexcitons in GaAs quantum wells. *Science* **324**, 1169–1173 (2009).
- [12] Turner, D. & Nelson, K. Coherent measurements of high-order electronic correlations in quantum wells. *Nature* **466**, 1089–1092 (2010).
- [13] Tollerud, J. O. & Davis, J. A. Optical analogue of 2D heteronuclear double-quantum NMR. *arXiv:1607.044* (2016).
- [14] Bristow, A. D., Karaiskaj, D., Dai, X. & Cundiff, S. T. All-optical retrieval of the global phase for two-dimensional Fourier-transform spectroscopy. *Opt. Express* **16**, 18017–18027 (2008).
- [15] Helbing, J. & Hamm, P. Compact implementation of Fourier transform two-dimensional IR spectroscopy without phase ambiguity. *J. Opt. Soc. Am. B* **28**, 171–178 (2011).
- [16] Moody, G. et al. Coherent coupling of excitons and trions in a photoexcited CdTe/CdMgTe quantum well. *Phys. Rev. Lett.* **112**, 097401 (2014).
- [17] Hao, K. et al. Coherent and incoherent coupling dynamics between neutral and charged excitons in monolayer MoSe₂. *Nano Letters* **16**, 5109–5113 (2016).
- [18] Moody, G. et al. Influence of confinement on biexciton binding in semiconductor quantum dot ensembles measured with two-dimensional spectroscopy. *Phys. Rev. B* **87**, 041304 (2013).
- [19] Moody, G. et al. Fifth-order nonlinear optical response of excitonic states in an InAs quantum dot ensemble measured with two-dimensional spectroscopy. *Phys. Rev. B* **87**, 045313 (2013).
- [20] Cassette, E., Dean, J. C. & Scholes, G. D. Two-dimensional visible spectroscopy for studying colloidal semiconductor nanocrystals. *Small* **12**, 2234–2244 (2016).
- [21] Langbein, W. & Patton, B. Microscopic measurement of photon echo formation in groups of individual excitonic transitions. *Phys. Rev. Lett.* **95**, 017403 (2005).
- [22] Fras, F. et al. Multi-wave coherent control of a solid state single emitter. *Nat. Phot.* **10**, 155 (2016).
- [23] Mermillod, Q. et al. Harvesting, coupling, and control of single-exciton coherences in photonic waveguide antennas. *Phys. Rev. Lett.* **116**, 163903 (2016).
- [24] Jakubczyk, T. et al. Impact of phonons on dephasing of individual excitons in deterministic quantum dot microlenses. *ACS Photonics* **3**, 2461–2466 (2016).
- [25] Maier, S. et al. Bright single photon source based on self-aligned quantum dot-cavity systems. *Opt. Express* **22**, 8136–8142 (2014).
- [26] Mermillod, Q. et al. Dynamics of excitons in individual InAs quantum dots revealed in four-wave mixing spectroscopy. *Optica* **3**, 377 (2016).
- [27] Kim, J., Mukamel, S. & Scholes, G. D. Two-dimensional electronic double-quantum coherence spectroscopy. *Accounts of Chemical Research* **42**, 1375–1384 (2009).
- [28] Karaiskaj, D. et al. Two-quantum many-body coherences in two-dimensional Fourier-transform spectra of exciton resonances in semiconductor quantum wells. *Phys. Rev. Lett.* **104**, 117401 (2010).
- [29] Turner, D. B., Wen, P., Arias, D. H. & Nelson, K. A. Coherent two-exciton dynamics measured using two-quantum rephasing two-dimensional electronic spectroscopy. *Phys. Rev. B* **84**, 165321 (2011).
- [30] Fingerhut, B. P., Richter, M., Luo, J.-W., Zunger, A. & Mukamel, S. 2D optical photon echo spectroscopy of a self-assembled quantum dot. *Ann. Phys.* **525**, 31 (2013).
- [31] Kasprzak, J. et al. Vectorial nonlinear coherent response of a strongly confined exciton-biexciton system. *New J. Phys.* **15**, 055006 (2013).
- [32] Langbein, W., Meier, T., Koch, S. & Hvam, J. Spectral signatures of $\chi^{(5)}$ processes in four-wave mixing of homogeneously broadened excitons. *J. Opt. Soc. Am. B* **18**, 1318 (2001).
- [33] Patton, B., Langbein, W., Woggon, U., Maingault, L. & Mariette, H. Time- and spectrally-resolved four-wave mixing in single CdTe/ZnTe quantum dots. *Phys. Rev. B* **73**, 235354 (2006).
- [34] Kasprzak, J., Patton, B., Savona, V. & Langbein, W. Coherent coupling between distant excitons revealed by two-dimensional nonlinear hyperspectral imaging. *Nat. Phot.* **5**, 57–63 (2011).

- [35] Abramavicius, D., Palmieri, B., Voronine, D. V., Sanda, F. & Mukamel, S. Coherent multidimensional optical spectroscopy of excitons in molecular aggregates; quasi-particle versus supermolecule perspectives. Chem. Rev. **109**, 2350–2408 (2009).
- [36] Specht, J. F., Knorr, A. & Richter, M. Two-dimensional spectroscopy: An approach to distinguish Förster and Dexter transfer processes in coupled nanostructures. Phys. Rev. B **91**, 155313 (2015).
- [37] Stinaff, E. A. et al. Optical signatures of coupled quantum dots. Science **311**, 636 (2006).
- [38] Ardel, P.-L. et al. Coulomb mediated hybridization of excitons in coupled quantum dots. Phys. Rev. Lett. **116**, 077401 (2016).
- [39] Kapfinger, S. et al. Dynamic acousto-mechanical control of a strongly coupled photonic molecule. Nat. Comm. **6**, 8540 (2015).
- [40] Albert, F. et al. Microcavity controlled coupling of excitonic qubits. Nat. Comm. **4**, 1747 (2013).

SUPPLEMENTARY MATERIAL

Coherent coupling of individual quantum dots measured with phase-referenced two-dimensional spectroscopy: photon echo versus double quantum coherence

Valentin Delmonte, Judith F. Specht, Tomasz Jakubczyk, Sven Höfling, Martin Kamp, Christian Schneider, Wolfgang Langbein, Gilles Nogues, Marten Richter, and Jacek Kasprzak

THEORY NOTES

The model system used for the quantum dot (QD) molecule is discussed and the third-order response function is derived. The Liouville space pathways entering the rephasing photon echo and non-rephasing double-quantum coherence signal are illustrated using double-sided Feynman diagrams [1]. Finally, the simulation parameters are given and the calculated spectra are discussed with respect to the coupling type of the QD molecule measured in Fig. 5 of the main manuscript.

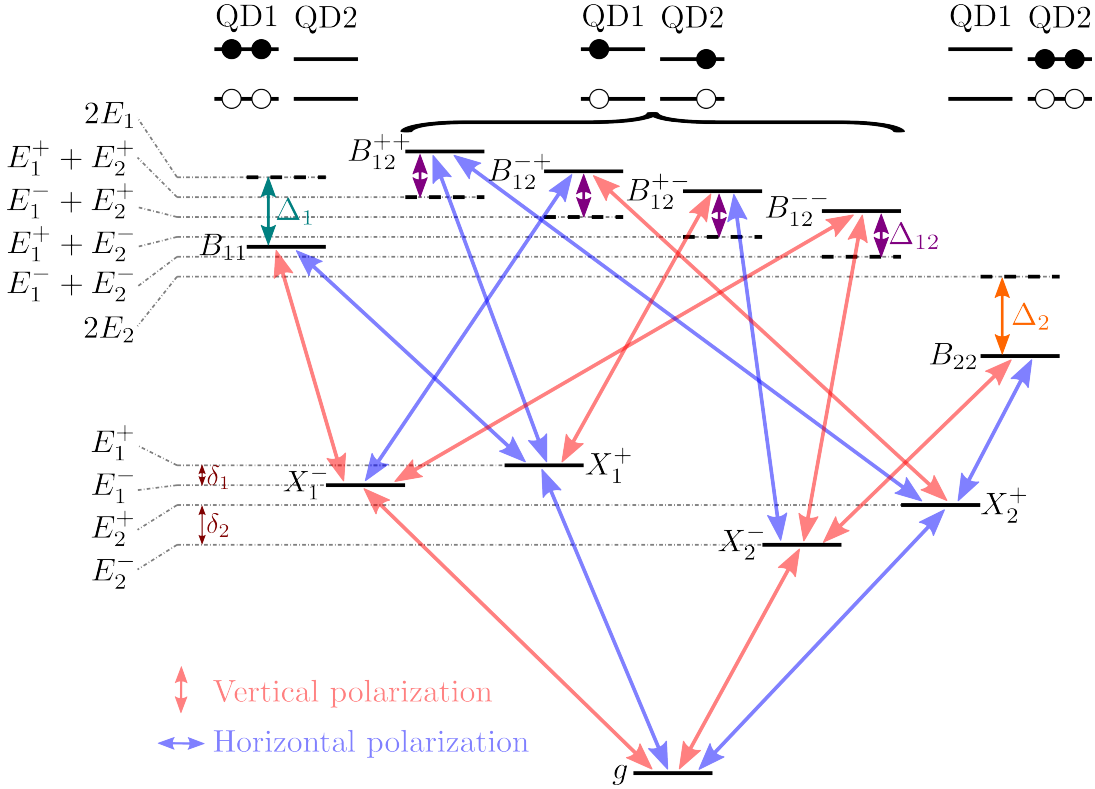
Model system of a quantum dot molecule

We will show that the signatures observed in the measured spectrum of Fig. 5 of the main text clearly indicate an intradot and interdot coupling of excitons in a quantum dot (QD) molecule consisting of two coupled QDs with resonance energies E_1 and E_2 , each with a different spin-orbit coupling δ_1 and δ_2 , respectively. The level scheme of such a QD molecule is schematically shown in Fig. S1. There, the electrostatic Coulomb coupling shifts the energy of the doubly excited states with respect to the single exciton energies of its constituents. Δ_1 (Δ_2) denotes the intradot biexciton shift within QD 1 (QD 2) and Δ_{12} represents the electrostatic interdot coupling between an exciton in QD 1 and an exciton in QD 2, forming a bound interdot biexciton B_{12} . The optical selection rules are governed by the fine-structure splitting (FSS): they originate from an exchange interaction between the two circularly polarized excitons in one QD, resulting in a new linearly polarized basis of excitonic eigenstates [2]. Vertically polarized optical excitations are marked with red arrows, horizontally polarized with blue arrows in Fig. S1. Since the resonances of the two exciton levels of each QD separated by the FSS are (more or less) equally pronounced in the measured spectrum, we assume an angle of 45° between the direction of the linear excitation/reference polarization and the fine-structure axis of the two dots in our theoretical calculation. This way, all interaction pathways shown in Fig. S1 contribute to the measured signal and a FSS will show up in the optical spectra.

Calculation of the rephasing photon echo and non-rephasing double-quantum coherence

In the following, the rephasing one-quantum and non-rephasing two-quantum signals are calculated following Ref. [1]. In a four-wave mixing (FWM) experiment in the $\chi^{(3)}$ regime, the applied optical field is composed of a sequence of three pulses with envelopes $\mathcal{E}_j^{u_j}$ (where $\mathcal{E}_j^{-1} = [\mathcal{E}_j^{+1}]^*$), frequencies $\tilde{\omega}_j$, and phases φ_j . Each pulse j is centered at time $\tilde{\tau}_j$:

$$(r, t) = \sum_{j=1}^3 \sum_{u_j=\pm 1} \mathcal{E}_j^{u_j}(r, t - \tilde{\tau}_j) e^{iu_j(\varphi_j - \tilde{\omega}_j(t - \tilde{\tau}_j))}. \quad (1)$$



Supplementary Figure S1. Schematic level scheme of a QD molecule consisting of two QDs. The exciton energies of the two QDs are E_1 and E_2 . Δ_{12} is the electrostatic coupling of a doubly excited state, if one exciton is present in every QD. Each QD exhibits a fine-structure splitting δ_i , which separates the QD excitons into an upper state $E_i^+ = E_i + \frac{\delta_i}{2}$ and a lower state $E_i^- = E_i - \frac{\delta_i}{2}$ ($i = 1, 2$). For our QD molecule, the intradot biexciton binding energies Δ_1 and Δ_2 shift the biexciton states B_{11} at energy $2E_1$ and B_{22} at energy $2E_2$ towards lower energies, whereas the interdot coupling is repulsive, i.e., shifts the B_{12} states towards higher energies.

The third-order response function links the polarization induced in the system to the applied electric field:

$$P_\alpha^{(3)}(r, t) = \int_0^\infty \int_0^\infty \int_0^\infty dt_3 dt_2 dt_1 \sum_{\beta, \gamma, \delta=1}^3 R_{\alpha\beta\gamma\delta}^{(3)}(t_3, t_2, t_1) \times E_\beta(r, t - t_3) E_\gamma(r, t - t_3 - t_2) E_\delta(r, t - t_3 - t_2 - t_1). \quad (2)$$

The heterodyned signal is a function of the delay times $\tau_{ij} \equiv \tilde{\tau}_j - \tilde{\tau}_i$ between the pulses:

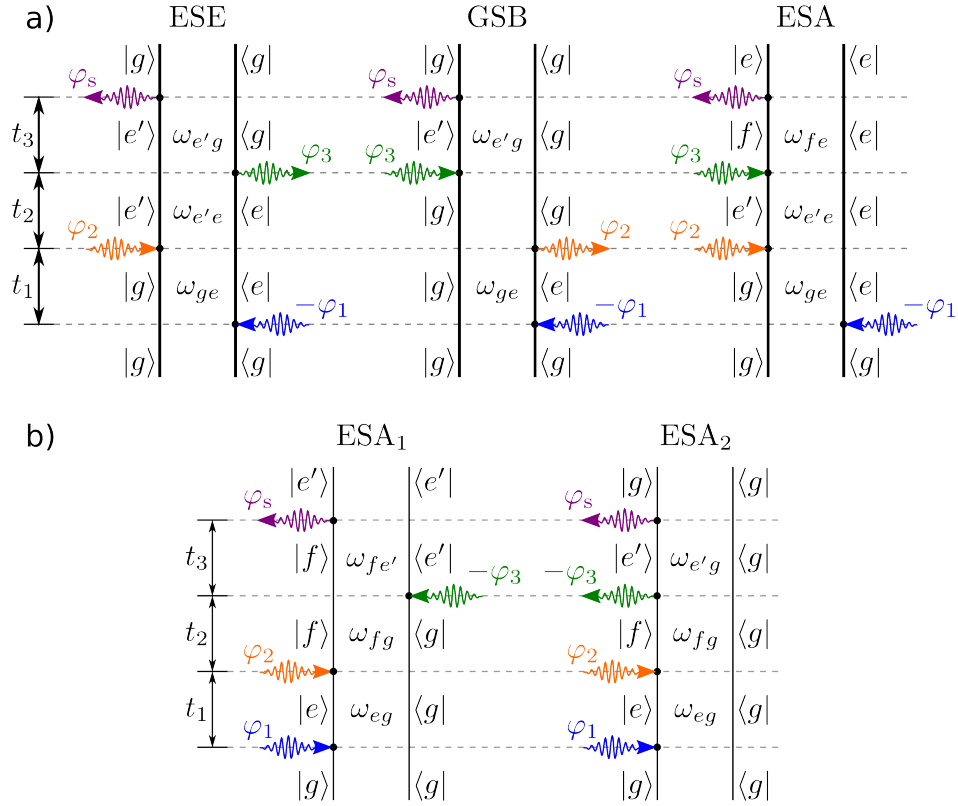
$$S_{\Omega_s}^{(3)}(\tau_{3s}, \tau_{23}, \tau_{12}) = \int_{-\infty}^{+\infty} dt P_{\Omega_s}(t) \cdot \mathcal{E}_s^*(t - \tilde{\tau}_s) e^{i\tilde{\omega}_s(t - \tilde{\tau}_s)}, \quad (3)$$

where $\mathcal{E}_s(t - \tilde{\tau}_s)$ denotes the local oscillator field envelope and $\Omega_s = u_1\Omega_1 + u_2\Omega_2 + u_3\Omega_3$ describes the specific phase combination of the detected signal.

The rephasing photon-echo (PE) frequency combination is $\Omega_s = \Omega_I = -\Omega_1 + \Omega_2 + \Omega_3$. There are three types of excitation quantum pathways contributing to the rephasing signal, denoted excited-state emission (ESE), ground-state bleaching (GSB), and excited-state absorption (ESA) and illustrated as double-sided Feynman diagrams in Fig. S2(a). The ESE and GSB pathway involve only the singly excited states e , whereas the ESA pathway includes also the doubly excited states f . Note that in the absence of many-body interactions, the two Liouville space pathways involving singly excited states (lower transitions) are completely canceled out by the pathway including the doubly excited states (upper transitions) for off-diagonal resonances and therefore, all off-diagonal peaks vanish [3, 4].

The non-rephasing double-quantum coherence (DQC) frequency combination is $\Omega_s = \Omega_{III} = +\Omega_1 + \Omega_2 - \Omega_3$. The signal has two contributing ESA pathways, cf. Fig. S2(b).

The rephasing PE one-quantum signal in frequency domain is calculated by Fourier transforming the third-order heterodyne-detected signal with respect to the time intervals t_1 and t_3 between the pulses. t_2 is fixed (In particular,



Supplementary Figure S2. Double-sided Feynman diagrams illustrating the Liouville space pathways of the density matrix evolution. They enter the rephasing one-quantum signal $\Omega_s = -\Omega_1 + \Omega_2 + \Omega_3$ (a) and the non-rephasing two-quantum signal $\Omega_s = +\Omega_1 + \Omega_2 - \Omega_3$ (b).

in the two-pulse FWM it is vanishing). The three contributions have the form [1]

$$S_{\text{ESE}}^{(3)}(\omega_3, \tau_2, \omega_1) = \frac{(2\pi)^4}{\hbar^3} \sum_{e, e'} (d_{e'g}^* \cdot \mathcal{E}_s^*(\omega_{e'g} - \tilde{\omega}_s)) (d_{e'g} \cdot \mathcal{E}_2(\omega_{e'g} - \tilde{\omega}_2)) e^{-i\xi_{e'e}t_2} \times \frac{d_{eg} \cdot \mathcal{E}_3(\omega_{eg} - \tilde{\omega}_3)}{\omega_3 - \xi_{e'g}} \frac{d_{eg}^* \cdot \mathcal{E}_1^*(\omega_{eg} - \tilde{\omega}_1)}{\omega_1 - \xi_{ge}}, \quad (4)$$

$$S_{\text{GSB}}^{(3)}(\omega_3, \tau_2, \omega_1) = \frac{(2\pi)^4}{\hbar^3} \sum_{e, e'} (d_{e'g}^* \cdot \mathcal{E}_s^*(\omega_{e'g} - \tilde{\omega}_s)) (d_{eg} \cdot \mathcal{E}_2(\omega_{eg} - \tilde{\omega}_2)) \times \frac{d_{e'g} \cdot \mathcal{E}_3(\omega_{e'g} - \tilde{\omega}_3)}{\omega_3 - \xi_{e'g}} \frac{d_{eg}^* \cdot \mathcal{E}_1^*(\omega_{eg} - \tilde{\omega}_1)}{\omega_1 - \xi_{ge}}, \quad (5)$$

$$S_{\text{ESA}}^{(3)}(\omega_3, \tau_2, \omega_1) = -\frac{(2\pi)^4}{\hbar^3} \sum_{e, e', f} (d_{fe}^* \cdot \mathcal{E}_s^*(\omega_{fe} - \tilde{\omega}_s)) (d_{e'g} \cdot \mathcal{E}_2(\omega_{e'g} - \tilde{\omega}_2)) e^{-i\xi_{e'e}t_2} \times \frac{d_{fe'} \cdot \mathcal{E}_3(\omega_{fe'} - \tilde{\omega}_3)}{\omega_3 - \xi_{fe}} \frac{d_{eg}^* \cdot \mathcal{E}_1^*(\omega_{eg} - \tilde{\omega}_1)}{\omega_1 - \xi_{ge}}, \quad (6)$$

where we defined $\xi_{ab} \equiv \omega_{ab} - i\gamma_{ab}$. d_{ab} denotes the dipole moment, ω_{ab} the resonance energy and γ_{ab} the homogeneous broadening of the $b \rightarrow a$ transition. The total rephasing PE signal is the sum of the three contributions:

$$S_{\text{PE}}^{(3)}(\omega_3, t_2, \omega_1) = S_{\text{ESE}}^{(3)}(\omega_3, t_2, \omega_1) + S_{\text{GSB}}^{(3)}(\omega_3, t_2, \omega_1) + S_{\text{ESA}}^{(3)}(\omega_3, t_2, \omega_1). \quad (7)$$

Similarly, the double-quantum signal is obtained by Fourier transforming the signal function with respect to the delay times t_2 and t_3 . It is composed of the two ESA pathways:

$$S_{\text{DQC}}^{(3)}(\omega_3, \omega_2, t_1) = S_{\text{ESA}_1}^{(3)}(\omega_3, \omega_2, t_1) + S_{\text{ESA}_2}^{(3)}(\omega_3, \omega_2, t_1) \quad (8)$$

with

$$S_{\text{ESA}_1}^{(3)}(\omega_3, \omega_2, t_1) = -\frac{(2\pi)^4}{\hbar^3} \sum_{e, e', f} (d_{fe'}^* \cdot \mathcal{E}_s^*(\omega_{fe'} - \tilde{\omega}_s)) (d_{eg} \cdot \mathcal{E}_1(\omega_{eg} - \tilde{\omega}_1)) e^{-i\xi_{eg}t_1} \times \frac{d_{e'g}^* \cdot \mathcal{E}_3^*(\omega_{e'g} - \tilde{\omega}_3)}{\omega_3 - \xi_{fe'}} \frac{d_{fe} \cdot \mathcal{E}_2(\omega_{fe} - \tilde{\omega}_2)}{\omega_2 - \xi_{fg}}, \quad (9)$$

$$S_{\text{ESA}_2}^{(3)}(\omega_3, \omega_2, t_1) = \frac{(2\pi)^4}{\hbar^3} \sum_{e, e', f} (d_{e'g}^* \cdot \mathcal{E}_s^*(\omega_{e'g} - \tilde{\omega}_s)) (d_{eg} \cdot \mathcal{E}_1(\omega_{eg} - \tilde{\omega}_1)) e^{-i\xi_{eg}t_1} \times \frac{d_{fe'}^* \cdot \mathcal{E}_3^*(\omega_{fe'} - \tilde{\omega}_3)}{\omega_3 - \xi_{e'g}} \frac{d_{fe} \cdot \mathcal{E}_2(\omega_{fe} - \tilde{\omega}_2)}{\omega_2 - \xi_{fg}}. \quad (10)$$

These signal functions enable us to calculate 2D maps of the rephasing and non-rephasing FWM pathways depending on the Fourier transformed pulse delays.

Model parameters

The parameters used to calculate the rephasing and non-rephasing 2D FWM spectra were chosen in agreement with the experimental data (see Supplementary Tab. I).

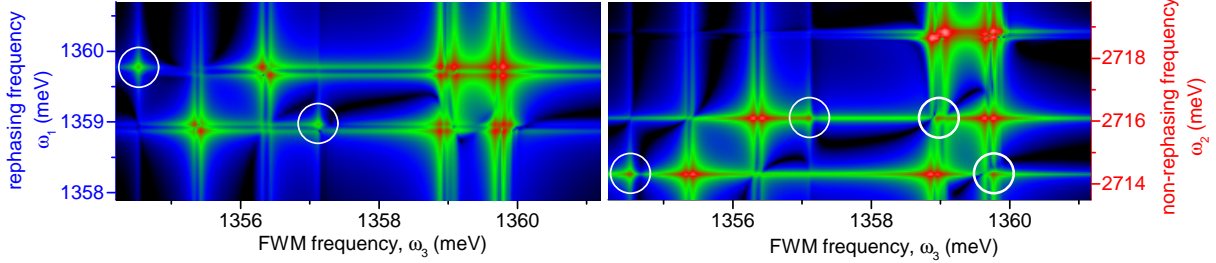
The homogeneous linewidth is typically in the order of few μeV , which corresponds to a dephasing time of few hundred picoseconds [5, 6]. Here, we choose $\gamma = 1/(500 \text{ ps})$ [7]. Moreover, the spectrometer resolution of $\sim 25 \mu\text{eV}$ was incorporated into the homogeneous linewidth for a quick estimation of its effect. The transition dipole moments of both QDs are chosen equally. Spectral wandering induces an inhomogeneous broadening [2] of $10 \mu\text{eV}$. This is included in the calculations by averaging the contributions to the signal functions for normally distributed values of the system resonances.

	QD 1	QD2
resonance energy	$E_1 = 1359.7 \text{ meV}$	$E_2 = 1358.95 \text{ meV}$
fine-structure splitting	$\delta_1 = 60 \mu\text{eV}$	$\delta_2 = 140 \mu\text{eV}$
biexciton binding energy	$\Delta_1 = -3.3 \text{ meV}$	$\Delta_2 = -3.6 \text{ meV}$
interdot coupling	$\Delta_{12} = +0.09 \text{ meV}$	

TABLE I. Model parameters used to calculate the optical response of the QD molecule composed of two coupled InAs QDs.

Evaluation of the spectra

Fig. 5 and of the main text shows the calculated one-quantum rephasing (a) and two-quantum non-rephasing (b) 2D spectra of the QD molecule specified by the parameters given in Sec. . As mentioned before, Coulomb interactions between the excited states cause that the doubly excited states are energetically shifted compared to the sum of the energies of the (isolated) single exciton constituents. This breaks the symmetry between the $G \rightarrow X$ and $X \rightarrow B$ transitions and leads to off-diagonal peaks in the rephasing 2D spectrum. In the measured spectrum in Fig. 5(a) of the main text, multiple off-diagonal peaks appear, indicating multiple exciton couplings. The spin-orbit coupling splits the exciton resonances of every QD, leading to four-peak clusters in the rephasing spectrum. Moreover, the upper X_2X_1 ($\omega_3 = E_2; \omega_1 = E_1$) and lower X_1X_2 ($\omega_3 = E_1; \omega_1 = E_2$) cross peaks form a square with the two GX_1 and GX_2 resonances at energies $E_1 = 1359.7 \text{ meV}$ and $E_2 = 1358.95 \text{ meV}$ on the diagonal. This pattern indicates an interdot exciton-exciton coupling between QD 1 and QD 2. (Without this coupling, these cross-peaks interfere destructively and cancel.) The electrostatic interdot coupling $\Delta_{12} = 0.09 \text{ meV}$ is small compared to the linewidth and spectrometer resolution. Thus, the corresponding interaction-shifted resonances cannot be identified as separate peaks in the spectrum, but as blueshifted high-energy shoulders of the exciton peaks, as explicitly depicted in Supplementary Fig. X. Finally, the off-diagonal X_1B_1 and X_2B_2 peaks at one-photon frequencies E_1 and E_2 are redshifted along the FWM axis by the intradot biexciton binding energies $\Delta_1 = -3.3 \text{ meV}$ in QD 1 and $\Delta_2 = -3.6 \text{ meV}$ in QD 2. In the two-quantum spectrum, the coupling of the two QDs leads to a peak pair labeled X_2B_{12} and X_1B_{12} at the



Supplementary Figure S3. Calculated rephasing one-quantum (a) and non-rephasing two-quantum (b) 2D FWM spectra including Förster coupling. The additional peaks arising due to exciton transfer processes between the QDs are marked by white circles.

interaction-shifted two-exciton transition GB_{12} at energy $\omega_2 = E_1 + E_2 + \Delta_{12}$ with FWM frequencies $\omega_3 = E_1$ and $\omega_3 = E_2$, respectively. Moreover, QD 1 (QD 2) forms a fine-structure split exciton-biexciton complex at two-photon frequency $2E_1 - |\Delta_1|$ ($2E_2 - |\Delta_2|$). The corresponding peak pairs are labeled GX_i and X_iB_i with $i \in 1, 2$.

A comparison of the measured and calculated spectra also shows that exciton energy transfer processes between the two quantum dots such as dipole-induced (Förster) interaction and Dexter-type coupling via wave-function overlap are negligible in the considered system: First, the corresponding coupling strengths in the order of μeV [4] are too small to be detected for the achieved spectrometer resolution. Second, the exciton transfer between the two QDs would lead to additional peaks at spectral positions where the second pulse creates a GB coherence involving an intradot biexciton in one QD before the third pulse induces a GX or XB coherence involving a single exciton in the other QD. To illustrate this, Suppl. Fig. S3 shows the calculated spectra including a (large) Förster coupling of 0.1 meV between the two QDs. The additional peaks arising due to interdot exciton transfer are highlighted by white circles.

This way, the analysis of the measured and calculated spectra enables us to identify the coupling type and strength, providing evidence of a QD molecule consisting of two electrostatically coupled QDs.

AUXILIARY EXPERIMENTAL RESULTS

Implementation of the phase-referencing protocol

In this section, we present the protocol which we established to reference the phase of the FWM signal by using the excitation pulses \mathcal{E}_1 and \mathcal{E}_2 . For all measured delays τ_{12} , before and after acquiring FWM signal at $2\Omega_2 - \Omega_1$ frequency, we measure heterodyne spectral interferences at Ω_1 and Ω_2 , allowing to measure the phase of \mathcal{E}_1 and \mathcal{E}_2 : φ_1 and φ_2 , by performing spectral interferometry. Passive stabilization of the setup turns out to be sufficient to maintain the phase stability for each τ_{12} during a typical acquisition time of ten seconds, as required here. If however phase drift is detected, the supplementary phase-reference data are interleaved in between the FWM acquisition to monitor phase variation and to correct for it.

In Fig. S4 a and b we present the spectrally resolved real part of the signal heterodyned at Ω_1 and Ω_2 , respectively. Here, $\tau_{R2} = 3\text{ ps}$ and remains fixed during the measurement, whereas τ_{12} (and thus also delay between \mathcal{E}_1 and \mathcal{E}_R , τ_{R1}) is scanned. As a result, φ_1 shows strong fluctuations, while φ_2 displays a slope of only 2π through the whole sequence.

In the next step, we test the performance of the phase correction routine described in the main text. In panels d) and e) we see that φ_1 and φ_2 can be aligned with respect to a chosen frequency of around 1360.1 meV.

We will now impose this externally determined correction onto the FWM data shown c). Specifically, the FWM is corrected by phase factors $-\varphi_1$ and $2\varphi_2$, which are retrieved from d) and e), respectively. The real part of the FWM, phase-corrected using such external referencing is shown in panel h). The FWM phase is directly linked with the one of \mathcal{E}_1 and \mathcal{E}_2 , which are now measured and provide the reference frame at which we synchronize the FWM. The accuracy of the phase-referencing is confirmed by formation of narrow peaks in 2D FWM displayed in panel k). For comparison, panel i) shows 2D FWM obtained after correcting the phase directly on the FWM data.

In Fig. S5 we present phase-referenced 2D FWM, obtained in the non-rephasing configuration, $\tau_{12} < 0$.

Single and double quantum 2D FWM of individual quantum dots in a low excitation regime

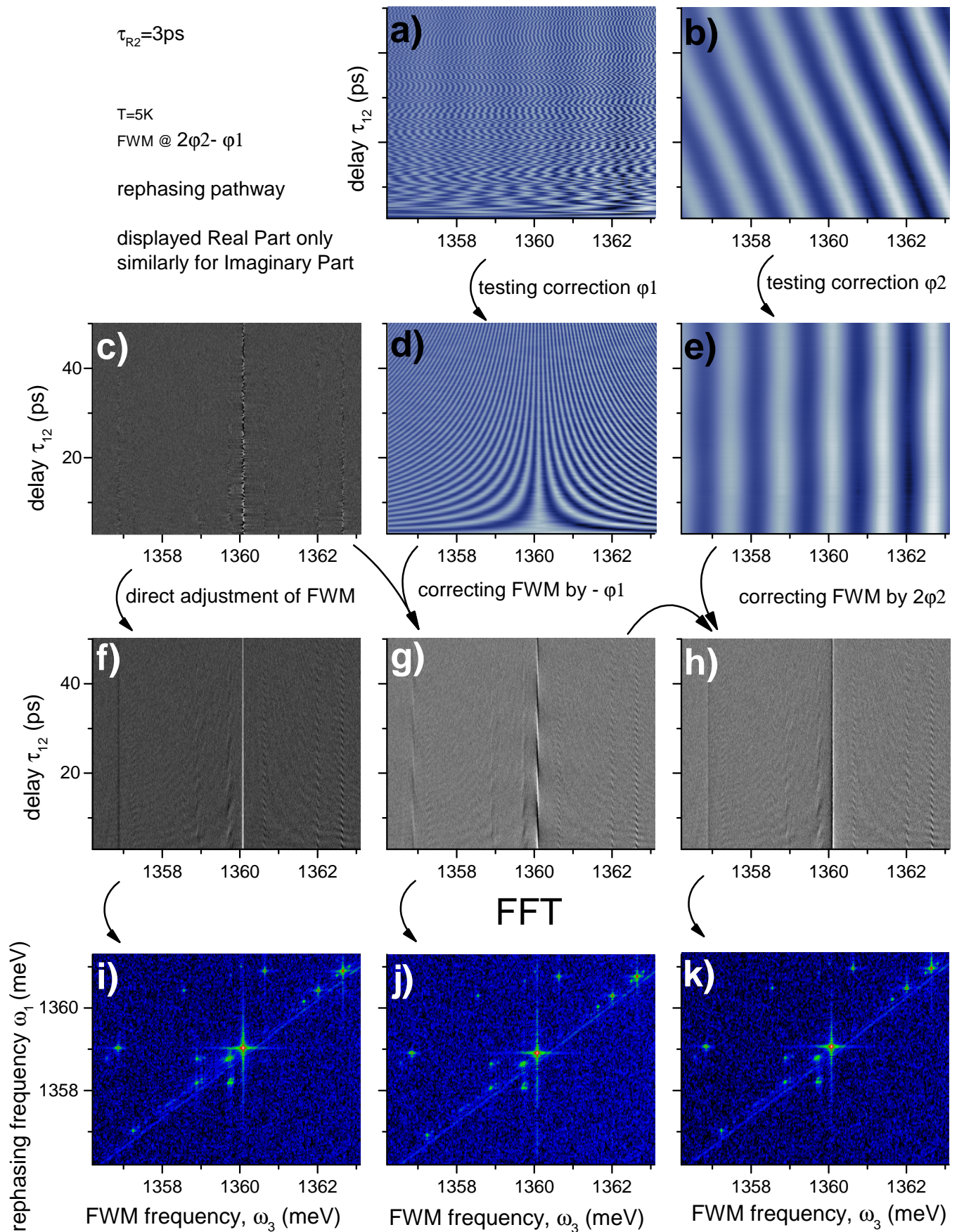
In Fig. S6 we present single (a) and double quantum (b) 2D FWM spectroscopy of individual QDs obtained under low excitation $\chi^{(3)}$ regime. The spectra reveal exciton-biexciton pairs, occurring in different QDs. In (a), the biexcitons are shifted from the excitons — placed at the diagonal (white line) $\omega_3 = \omega_1$ — by their binding energies of -0.7 meV (white dotted line), -3.3 meV (orange dashed line), -3.55 meV (green dash-dotted line). We note that, in contrast to the data shown in Fig. 4 a of the main manuscript, the signatures of biexcitons do not show up on the diagonal. This means the ground state-to-biexciton transitions are now not excited by \mathcal{E}_1 , confirming the low excitation regime. By inspecting the exciton-biexciton pair at (1360.67, 1357.1) meV we observe that, in the rephasing configuration, the FWM amplitude of the biexciton is an order of magnitude weaker than the exciton's one. Instead, in the non-rephasing situation the amplitude of both transitions is equal. Such a suppression of biexciton transition in the rephasing case is characteristic for transitions exhibiting a large inhomogeneous broadening (here around 0.2 meV, an order of magnitude larger than typically observed in this sample), and has been previously noticed in FWM of GaAs quantum wells [8]. Two other transitions, with an order of magnitude lower inhomogeneous broadening, show a textbook behavior with the exciton's amplitude twice stronger than (equal to) the biexciton in the rephasing (non-rephasing) configuration [2, 9].

Experimental insight into a QD molecule: FWM amplitude and phase, and hyperspectral imaging

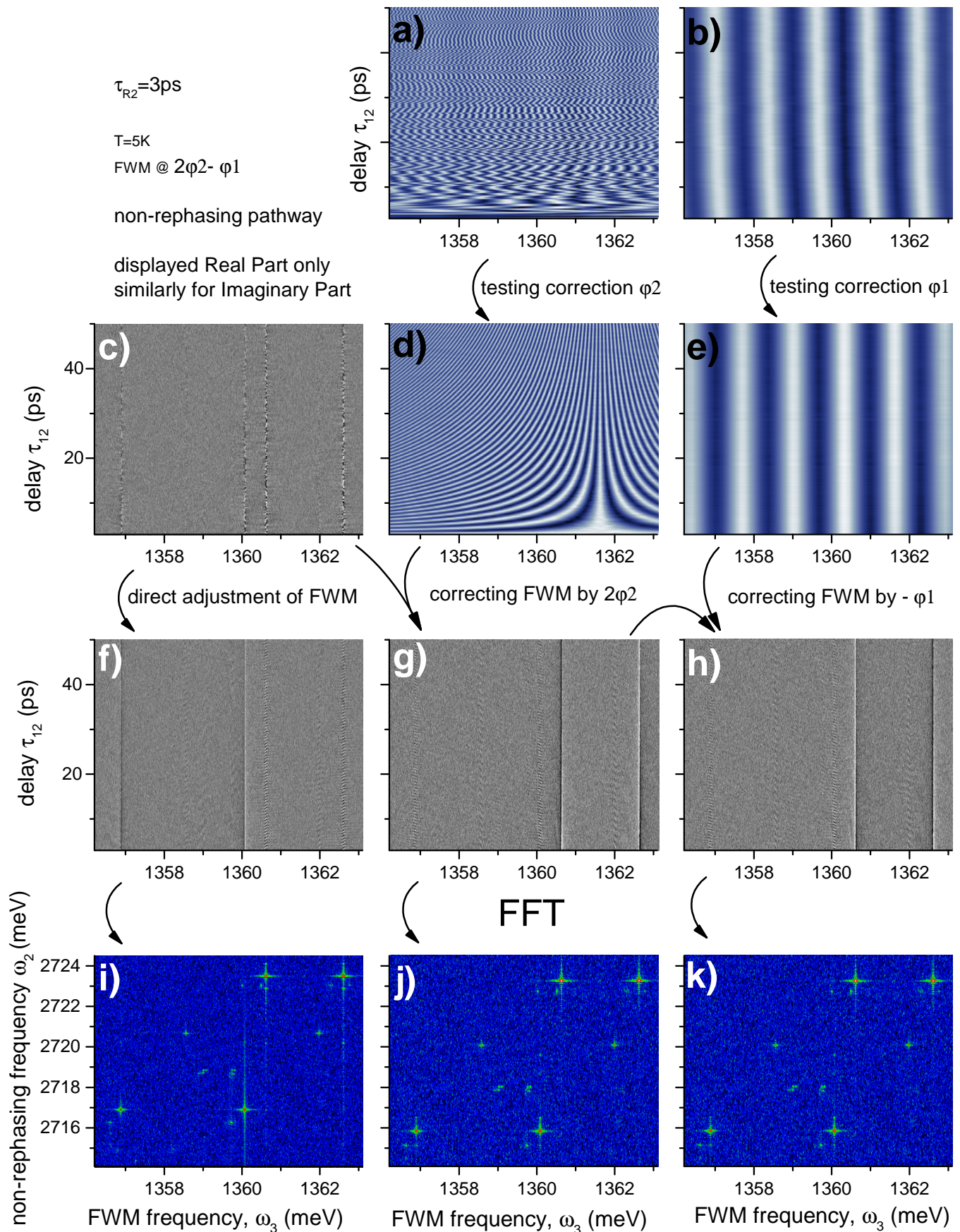
To better illustrate coherent coupling measured at the QD molecule investigated in Fig. 5 of the main manuscript, in Fig. S7 we present FWM amplitude (black traces) and phase (orange traces), retrieved from intersections through the 2D FWM spectrum in the rephasing configuration. The diagonal peaks display fine-structure splitting and overall phase shift of π over the resonances. The amplitude of off-diagonals show additional contributions, in agreement with simulations shown in Fig S8. Each off-diagonal peak pair exhibits a high-energy shoulder that is blueshifted by the interdot biexciton binding energy $\Delta_{12} = 90 \mu\text{eV}$. This lifts the degeneracy of the GX_1 (GX_2) and X_2B_{12} (X_1B_{12}) contributions, such that they do not coincide spectrally and therefore do not cancel each other out. We also observe a 2π phase shift across the off-diagonals, indicating electrostatic coupling resulting in the biexciton blueshift [4, 10]. Note that the phase shifts across the off-diagonals in the theoretical spectrum differ quantitatively from the measured ones, since here the FSS is resolved better than in the measured spectrum. On the other hand, the overlap with neighboring peaks has a stronger impact in the calculated spectrum (due to the Lorentzian form of the resonances), leading to phase interferences. As expected, both QDs are spatially co-localized with a few hundreds of nm, as confirmed by the FWM hyperspectral imaging. They are simultaneously excited by the laser spot (focussed down to the diffraction limit of around $0.85 \mu\text{m}$) positioned at the crossing point of blue lines.

* jacek.kasprzak@neel.cnrs.fr

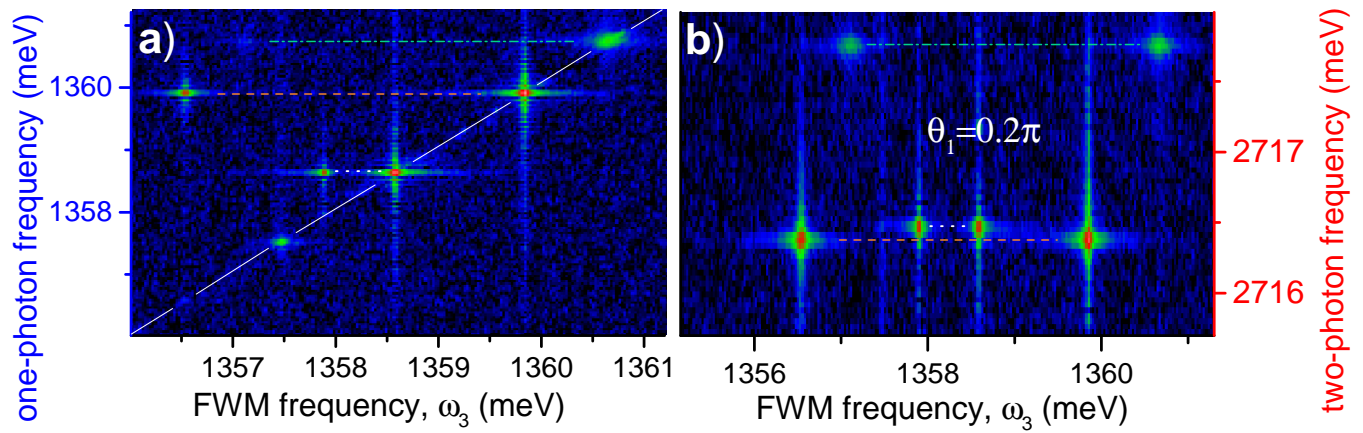
- [1] Abramavicius, D., Palmieri, B., Voronine, D. V., Sanda, F. & Mukamel, S. Coherent multidimensional optical spectroscopy of excitons in molecular aggregates; quasiparticle versus supermolecule perspectives. *Chem. Rev.* **109**, 2350–2408 (2009).
- [2] Mermillod, Q. et al. Dynamics of excitons in individual inas quantum dots revealed in four-wave mixing spectroscopy. *Optica* **3**, 377 (2016).
- [3] Dai, X. et al. Two-dimensional double-quantum spectra reveal collective resonances in an atomic vapor. *Phys. Rev. Lett.* **108**, 193201 (2012).
- [4] Kasprzak, J., Patton, B., Savona, V. & Langbein, W. Coherent coupling between distant excitons revealed by two-dimensional nonlinear hyperspectral imaging. *Nat. Phot.* **5**, 57–63 (2011).
- [5] Stock, E. et al. Acoustic and optical phonon scattering in a single In(Ga)as quantum dot. *Phys. Rev. B* **83**, 041304 (2011).
- [6] Ostapenko, I. A. et al. Exciton acoustic-phonon coupling in single GaN/AlN quantum dots. *Phys. Rev. B* **85**, 081303 (2012).
- [7] Borri, P. et al. Ultralong dephasing time in ingaas quantum dots. *Phys. Rev. Lett.* **87**, 157401 (2001).
- [8] Langbein, W. & Hvam, J. M. Biexcitonic bound and continuum states of homogeneously and inhomogeneously broadened exciton resonances. *phys. stat. sol. (a)* **190**, 167–174 (2002).
- [9] Kasprzak, J. et al. Vectorial nonlinear coherent response of a strongly confined exciton-biexciton system. *New J. Phys.* **15**, 055006 (2013).
- [10] Kasprzak, J. & Langbein, W. Coherent response of individual weakly confined exciton-biexciton systems. *J. Opt. Soc. Am. B* **29**, 1766–1771 (2012).



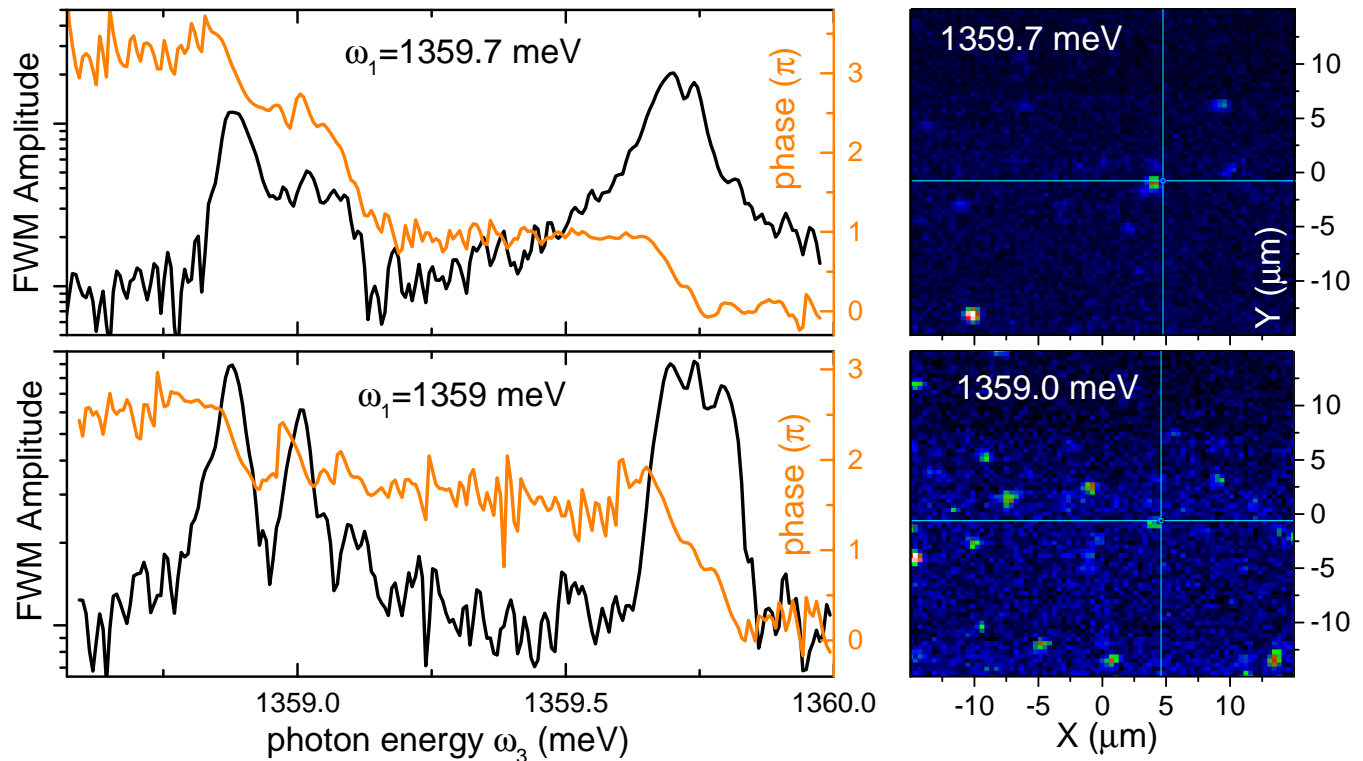
Supplementary Figure S4. **Phase-referencing protocol. Rephasing pathway.** (a, b, c) Spectrally-resolved heterodyne signal at Ω_1 , Ω_2 and $2\Omega_2 - \Omega_1$ respectively. (d, e, f) Phase-correction applied on (a, b, c), respectively. (g, h) Phase-correcting FWM data (c), using (d, e), respectively. (i, j, k) 2D FWM retrieved from (f, g, h), respectively. Only the real part of the data displayed. The correction is analogously applied to the imaginary part, which is not shown here.



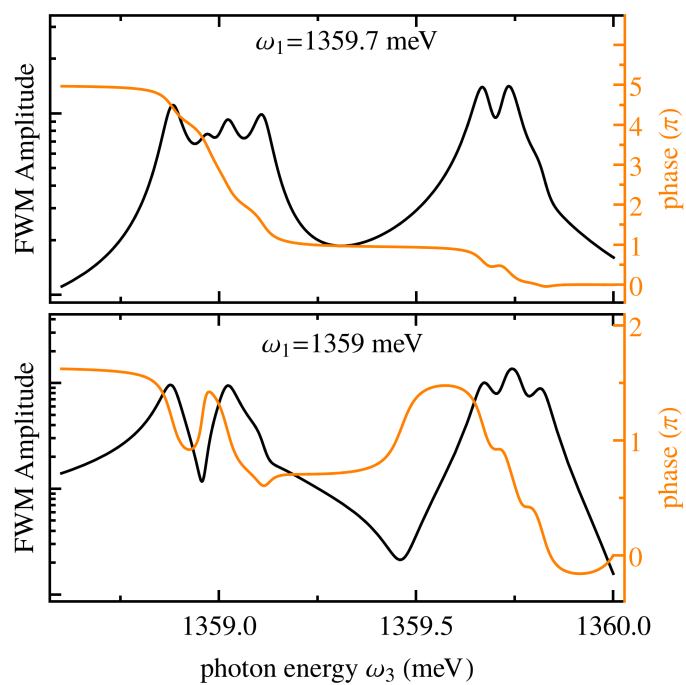
Supplementary Figure S5. **Phase-referencing protocol. Non-rephasing pathway.** (a, b, c) Spectrally-resolved heterodyne signal at Ω_2 , Ω_1 and $2\Omega_2 - \Omega_1$ respectively. (d, e, f) Phase-correction applied on (a, b, c), respectively. (g, h) Phase-correcting FWM data (c), using (d, e), respectively. (i, j, k) 2D FWM retrieved from (f, g, h), respectively. The correction is analogously applied to the imaginary part, which is not shown here.



Supplementary Figure S6. **2D FWM spectroscopy excitation-biexciton systems in three distinct InAs QDs in a low excitation regime.** (a) Rephasing, one-photon configuration. White line depicts the diagonal $\omega_3 = \omega_1$. (b) non-rephasing, two-photon configuration. The applied pulse areas of \mathcal{E}_1 and \mathcal{E}_2 was $(\theta_1, \theta_2) \simeq (0.2, 0.6)\pi$, co-linear polarization. The amplitude in logarithmic color scale over 2 orders of magnitude.



Supplementary Figure S7. **Amplitude and phase analysis retrieved from the 2D FWM shown in Fig. 5 a of the main manuscript and spatial location of coupled resonances forming a QD molecule.**



Supplementary Figure S8. Calculated amplitude and phase analysis, to be compared with the measured ones shown in Fig. S7.